Non-Markovian route to coherence in heterogeneous diffusive systems

Aranyak Sarkar [*]
Experimental Physics I, University of Bayreuth, Universitätsstr. 30, 95447 Bayreuth, Germany and Radiation & Photochemistry Division, Bhabha Atomic Research Centre, Mumbai 400085, India

(Received 28 April 2025; revised 10 July 2025; accepted 27 October 2025; published 12 November 2025)

Temporal coherence—persistent alignment across time—can arise between agents with fundamentally distinct dynamics, yet classical diffusion models (Brownian motion, fractional Brownian motion, generalized Langevin equations with shared noise) struggle under strong heterogeneity and asymmetry. We introduce the coupled memory graph process (CMGP), in which internal memory and directed, distance-gated coupling jointly produce synchronized behavior without reciprocity or common noise. Crucially, CMGP exhibits long-time coherence that reaches far beyond typical inherent memory times: an active particle with long-range memory remains temporally coherent with a subdiffusive partner despite mismatched scaling exponents. We show that this persistence arises from emergent long-range correlations generated by the coupling field rather than direct kernel overlap. Using Bayesian optimization, we identify broad parameter regions that support this "ghost coherence" (coherence without trajectory convergence) while preserving distinct exponents. These results outline a minimal mechanism for coordination in heterogeneous active systems and viscoelastic environments—one that standard stochastic models do not capture under comparable asymmetry unless augmented with explicit common drives or symmetric couplings.

DOI: 10.1103/6r83-n97h

I. INTRODUCTION

Stochastic dynamics underpin a wide range of processes in physics, biology, and soft matter—from intracellular organelle transport to stress relaxation in polymer networks and fluctuating flows in active media. Classical models such as Brownian motion (BM) and the Langevin equation have long served as foundational tools for describing such random motion. Yet, experimental observations across diverse systems reveal significant deviations from purely Markovian behavior, including memory effects, heterogeneous diffusivity, and environment-mediated feedback [1–9]. These findings challenge models that assume time-local, homogeneous noise and call for frameworks that can capture temporal persistence, cross trajectory influence, and emergent correlations in nonequilibrium media.

To capture temporal correlations, models such as fractional Brownian motion (FBM) impose power-law scaling in the displacement autocorrelation, typically written as $\langle x(t)x(t+\tau)\rangle \sim \tau^{2H}$, where H is the Hurst exponent [10,11]. The generalized Langevin equation (GLE) introduces memory via convolution with a friction kernel $\Gamma(t)$, yielding the integrodifferential form

$$m\ddot{x}(t) + \int_0^t \Gamma(t-s)\dot{x}(s)\,ds = \xi(t), \tag{1}$$

where $\xi(t)$ denotes correlated thermal noise [12,13]. While these models capture long-time correlations, they remain fundamentally trajectory local—each particle evolves independently, without intertrajectory feedback.

Other non-Markovian frameworks—such as aging fractional dynamics, power-law viscoelastic GLEs, and generalized continuous-time random walks—have extended memory descriptions [6,12,14,15], yet still lack a mechanism for directional coupling between distinct entities.

This limitation becomes critical in structured, dynamic environments. In active biological media, for instance, motor-driven cargo deforms the viscoelastic matrix, which in turn modulates neighboring particles through stress propagation [16]. These interactions are inherently asymmetric and time lagged: the conditional expectation $\langle \Delta x_i(t)\Delta x_j(t+\tau)\rangle$ can be significant even when the reverse is negligible, violating temporal reciprocity [17] and challenging classical memory-based models.

Furthermore, biological and soft-matter systems exhibit heterogeneous dynamics: subdiffusion, active bursts, and intermittent trapping may coexist within the same domain [18–21]. A physically meaningful model must therefore allow for particles with distinct noise amplitudes σ_i, memory kernels $\Theta_i(\tau)$, and diffusivity exponents α_i—yet remain capable of generating persistent cross correlations. Such interactions are captured by structured coherence functions of the form:

$$\phi_{ij}(\tau) = \langle \Delta x_i(t)\Delta x_j(t+\tau)\rangle - \langle \Delta x_i(t)\rangle\langle \Delta x_j(t+\tau)\rangle. \tag{2}$$

Here, $\Delta x_i(t) = x_i(t+\Delta t) - x_i(t)$ denotes the velocity increment of particle i, and the angle brackets $\langle\cdot\rangle$ represent a temporal average over t.

While composite-kernel GLEs and aging models partially address temporal heterogeneity [14,15], they treat memory

[*]Contact author: Aranyak.Sarkar@uni-bayreuth.de; aranyak@barc.gov.in

as an intrinsic, symmetric property of isolated trajectories. Consequently, they fail to account for emergent phenomena such as asymmetric feedback, spatiotemporal coherence, and environmentally mediated cross trajectory influence [22,23]. Mechanically coupled GLEs [13,24,25] (MechGLE) can generate alignment through shared viscoelastic baths, yet typically assume symmetric springlike couplings and require similar diffusive states for coherence to persist. Indeed, generalized Langevin frameworks have been extended to include interparticle memory coupling [26,27] and even nonreciprocal interactions [28]. However, these approaches usually impose reciprocal or common-noise coupling, and hence cannot sustain long-term coherence without eventually homogenizing the dynamics of all particles. These constraints reflect Onsager reciprocity [17], which enforces time-reversal symmetry and equal cross response coefficients near equilibrium. Systems that exhibit nonreciprocal coherence—such as active cytoplasmic transport—thus demand stochastic models that permit asymmetry in both memory and interactions [7,16]. Experiments have indeed revealed micron-scale coherent motion of chromatin in cell nuclei despite a viscoelastic environment [29], coexisting with strongly subdiffusive telomere dynamics [30], and peroxisomal transport in the cytoplasm similarly combines directed motion with subdiffusive fluctuations [31]. These observations exemplify the coexistence of activelike coherence and heterogeneous diffusion that motivates the asymmetric memory coupling in our model.

II. COUPLED MEMORY GRAPH PROCESS (CMGP) FRAMEWORK

We introduce the coupled memory graph process (CMGP), a general framework for modeling coherence between diffusively distinct agents through heterogeneous memory and asymmetric coupling. In this framework, each agent is represented as a node on a directed graph, where self-loops encode internal memory structure and directed edges mediate nonreciprocal, temporally filtered interactions.

The dynamics of agent $x_i(t)$ are governed by a non-Markovian integrodifferential equation:

$$\frac{dx_i(t)}{dt} = \int_0^t \Theta_i(t-s)\,\xi_i(s)\,ds + \sum_{j\neq i}\int_0^t \Phi_{ij}(t,s)\,K_{ij}(d_{ij}(s))\,ds + \eta_i(t), \qquad (3)$$

where

(1) $\Theta_i(t)$ is a memory kernel defining the temporal structure of internal stochastic input;

(2) $\xi_i(t)$ is independent Gaussian white noise, $\langle\xi_i(t)\xi_j(t')\rangle = \delta_{ij}\delta(t-t')$;

(3) $\Phi_{ij}(t,s)$ is s time-asymmetric influence kernel from agent j to i;

(4) $K_{ij}(d)$ is distance-dependent gain modulated by inter-agent distance $d_{ij}(s) = \|x_i(s) - x_j(s)\|$;

(5) $\eta_i(t)$ is additional uncorrelated white noise, $\langle\eta_i(t)\eta_j(t')\rangle = \sigma_\eta^2\delta_{ij}\delta(t-t')$.

The self-memory term,

$$\zeta_i(t) := \int_0^t \Theta_i(t-s)\,\xi_i(s)\,ds,$$

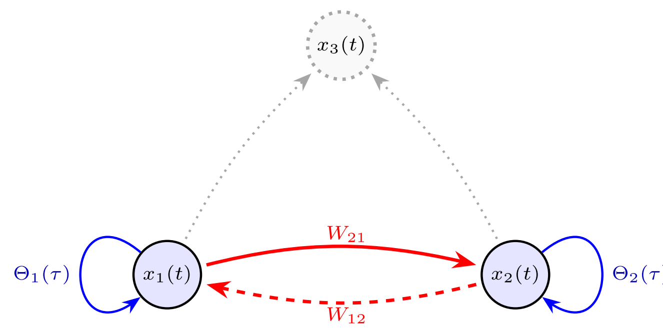

FIG. 1. Schematic representation of coupled memory graph process(CMGP). Nodes $x_i(t)$ carry self-memory $\Theta_i(\tau)$ (blue loops). A directed coupling $j \to i$ has effective edge weight $W_{ij}(t,\tau) = \Phi_{ij}(t,\tau)\,K_{ij}(t)$, where $\Phi_{ij}(t,\tau)$ is the lag kernel filtering past increments of x_j and $K_{ij}(t) = \kappa_{ij}\exp[-d_{ij}(t)/R_{ij}]$ with $d_{ij}(t) = \|x_i(t) - x_j(t)\|$. Bold red arrows mark the couplings actually used in our analyses (shown as W_{21} for the asymmetric case); dashed red arrows indicate an optional reciprocal pathway not included in the results (we set $\kappa_{12} = 0$ unless explicitly stated). The dotted gray node $x_3(t)$ and dotted gray arrows indicate network extendability ($N > 2$) and are not analyzed here.

defines a colored noise process with long-range temporal correlations. Its two-point correlation function is

$$\langle\zeta_i(t)\,\zeta_j(t')\rangle = \delta_{ij}\int_0^{\min(t,t')} \Theta_i(t-s)\,\Theta_i(t'-s)\,ds, \qquad (4)$$

which ensures stationarity and allows memory tuning via the kernel $\Theta_i(t)$.

Unlike classical generalized Langevin equation (GLE) models, where memory enters via frictional drag on past velocities (obeying fluctuation-dissipation relations), the CMGP formulation introduces nonequilibrium memory through convolution of white noise with a memory kernel. This construction imparts temporally correlated dynamics without requiring velocity damping or thermodynamic balance. Similar approaches have been employed in fractional Gaussian noise models, adaptive stochastic systems, and active media driven by structured fluctuations [32,33].

This formalism allows each agent to maintain a distinct internal memory profile (via Θ_i), while receiving directed, temporally filtered input (via Φ_{ij}) from other agents. The combination of noise-based memory and asymmetric coupling enables the emergence of persistent coherence between diffusively distinct agents—a phenomenon not captured by symmetric models such as MechGLE or shared-noise GLEs [34].

This formalism maps directly onto Fig. 1, where each node $x_i(t)$ integrates its own memory (via Θ_i, shown as blue self-loops) and receives delayed, distance-weighted input from others (via $\Phi_{ij}\cdot K_{ij}$, red arrows). The coupling is inherently asymmetric—since $\Phi_{ij} \neq \Phi_{ji}$—enabling directional coordination even across mismatched diffusivities.

By intentionally violating Onsager reciprocity [17], CMGP captures nonequilibrium dynamics inaccessible to classical models. Beyond pairwise interactions, it extends naturally to structured environments—such as deformable boundaries or viscoelastic fields—where memory-driven coupling with the medium produces long-range coherence. In such contexts, CMGP offers a flexible platform for modeling emergent, feedback-sensitive transport in soft and active matter.

III. MINIMAL TWO-PARTICLE MODEL

To understand how coherence emerges in complex networks of interacting agents, it is instructive to begin with the simplest nontrivial case: a two-particle system. This minimal setup captures the core mechanism of directionally coupled, memory-driven interactions while remaining analytically and computationally tractable.

We demonstrate the CMGP framework using a confined two-particle system in two-dimensional space, where particles A and B exhibit distinct diffusive behaviors. Particle A is active, influenced both by its own memory and by input from particle B. In contrast, particle B is passive, evolving solely under its intrinsic memory without external input. This setup directly corresponds to the schematic shown in Fig. 1: each particle integrates its own past through a self-memory kernel $\Theta(\tau)$ (illustrated by blue loops). Additionally, particle A receives history-dependent, distance-modulated input from particle B via a coherence kernel $\Phi(\tau)$ weighted by the spatial gain function $K(d_{AB}(t))$ (represented by a red arrow).

Unlike classical models where symmetry or feedback ensures convergence, the interaction here is explicitly asymmetric: particle B influences A, but not vice versa. This configuration enables us to test the central premise of CMGP: can directional, memory-mediated coupling induce persistent temporal coherence in the presence of vast diffusive heterogeneity?

Inspired by the Volterra framework for systems with memory [35], we express the discrete-time update rules for CMGP as

$$x_A(t+1) = x_A(t) + \sum_{\tau=1}^{M} \Theta(\tau)\,\xi_A(t-\tau) + K(d_{AB}(t)) \sum_{\tau=1}^{M} \Phi(\tau)\,\Delta x_B(t-\tau) + \eta_A(t), \quad (5)$$

$$x_B(t+1) = x_B(t) + \sum_{\tau=1}^{M} \Theta(\tau)\,\xi_B(t-\tau) + \eta_B(t). \quad (6)$$

Here, the term $\Delta x_B(t-\tau) = x_B(t-\tau+1) - x_B(t-\tau)$ denotes the past displacement of particle B at lag τ, capturing the temporally resolved directed influence encoded by the memory kernel $\Phi(\tau)$.

The CMGP model is governed by two key parameters: the coupling strength κ and the memory depth M. The coupling strength κ determines the magnitude of interparticle alignment, while M controls how much of each particle's past trajectory is integrated into its current update.

Spatial interactions are modulated by a distance-dependent gain function,

$$K(d) = \kappa\, \exp\left(-\frac{d}{R}\right),$$

where R is a characteristic interaction radius that sets the spatial decay scale of the coupling. This exponential form reflects biophysical attenuation mechanisms such as elastic stress propagation or chemical signaling. While we focus on this exponential kernel, other monotonic forms (e.g., power law) yield qualitatively similar behavior.

Note that in Eq. (3), the coupling term $K(d_{AB}(t))$ is placed inside the memory sum to indicate its possible time dependence across all τ. However, in subsequent simplified formulations [e.g., Eq. (5)], we move $K(d_{AB}(t))$ outside the sum, assuming that the spatial separation varies slowly over the memory horizon or that the present distance dominates the feedback. This change is a modeling simplification and does not alter the essential dynamics when such assumptions hold.

Temporal memory is modeled using power-law decaying kernels for both self-memory and cross memory: $\Theta(\tau) = (\tau+1)^{-\alpha_m}$ and $\Phi(\tau) = (\tau+1)^{-\gamma_c}$, where $\alpha_m, \gamma_c \in (0,1)$ control the decay of self- and coherence memory, respectively. These forms reflect long-range temporal correlations observed in subdiffusive, viscoelastic, and active systems. While the exponents α_m and γ_c shape the decay profile of the memory (governing how past events are weighted), we impose a finite memory depth M to ensure physical realism and numerical stability. In real systems, memory is inherently limited by structural relaxation or environmental turnover, and for $\alpha_m \leqslant 1$, unbounded kernels can produce divergent integrals. Hence, α_m controls the temporal persistence of correlations, while M serves as a cutoff time scale beyond which memory is no longer retained.

IV. KEY OBSERVABLES

The core idea of the CMGP framework is to introduce directionally biased, memory-driven interactions—unlike classical models such as Brownian motion (BM), fractional Brownian motion (FBM), or generalized Langevin equations (GLE), which either lack interparticle coupling or rely on symmetric feedback (as in MechGLE). These asymmetric pathways enable particles to remain temporally synchronized without requiring convergence in their diffusive behaviors. To quantitatively assess this behavior, we define three core descriptors. The time-averaged mean squared displacement (TA-MSD) for particle i is defined as

$$\left\langle \delta_i^2(\tau) \right\rangle = \langle (x_i(t+\tau) - x_i(t))^2 \rangle_t,$$

which quantifies the typical squared displacement over a lag time τ, averaged over the full trajectory. To characterize the lag-dependent dynamical behavior, we compute the local diffusion exponent

$$\alpha_i(\tau) = \frac{d \log_{10} \left\langle \delta_i^2(\tau) \right\rangle}{d \log_{10} \tau},$$

which reflects how the TA-MSD scales with lag time at each τ. Transient fluctuations in $\alpha_i(\tau)$ reveal short-time dynamical variations, while the asymptotic limit $\tau \to \infty$ approaches $\alpha_i(\tau) \to 2H_i$, where H_i denotes the effective Hurst exponent. This long-time exponent characterizes the true diffusive state of the particle. Temporal coherence is quantified by the normalized cross correlation $C_{AB}(\tau) = \frac{\langle \Delta x_A(t,\tau)\, \Delta x_B(t,\tau) \rangle_t}{\sqrt{\langle \Delta x_A^2(t,\tau) \rangle_t \langle \Delta x_B^2(t,\tau) \rangle_t}}$, where $\Delta x_i(t,\tau) = x_i(t+\tau) - x_i(t)$. The CMGP model uniquely supports the coexistence of high temporal coherence and persistent diffusive disparity. This regime—marked by elevated $C_{AB}(\tau)$ and sustained differences

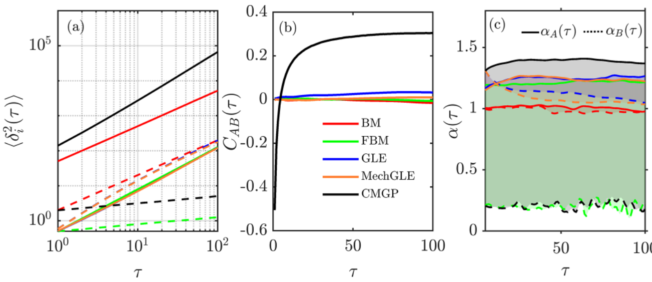

FIG. 2. Quantitative comparison of two-particle dynamics under five models: Brownian motion (BM), fractional Brownian motion (FBM), generalized Langevin equation (GLE) with shared noise, symmetrically coupled MechGLE, and asymmetrically coupled CMGP. All simulations use a memory depth of $M = 10$ and a cross coupling strength of $\kappa = 3$ (where applicable). All simulations use a memory depth of $M = 10$ and a cross coupling strength of $\kappa = 3$ (where applicable). Results are computed after a warm-up period of 200 steps to ensure steady-state behavior. (a) Time-averaged MSD curves for particles A (solid) and B (dashed) show strong convergence in MechGLE and GLE (due to symmetric coupling or shared noise), but persistent disparity in CMGP. (b) Temporal coherence $C_{AB}(\tau)$, calculated using the normalized Pearson-style cross correlation, is negligible for BM and FBM, modest in GLE and MechGLE, and sustained at long times in CMGP. The low coherence in MechGLE here reflects a specific regime of moderate memory mismatch and weak coupling, selected to preserve dynamical disparity. (c) Local diffusion exponents $\alpha_A(\tau)$ (solid) and $\alpha_B(\tau)$ (dashed) show that MechGLE and GLE enforce asymptotic convergence of particle behavior, while CMGP maintains distinct exponents—demonstrating the hallmark of persistent ghost coherence.

in $\alpha_i(\tau)$—defines the emergent phenomenon of ghost coherence, where particles are "in sync" in time without mirroring each other's trajectories, a feature absent in conventional stochastic models, which invariably require convergence of dynamics to achieve long-term correlations. In CMGP, both $C_{AB}(\tau)$ and the local exponents $\alpha_i(\tau)$ saturate at long lag times (extending well beyond the memory depth M), confirming that alignment is sustained beyond the nominal memory horizon. Note that all variables in this study are expressed in dimensionless units to highlight universal dynamical features, independent of specific material parameters. Time is measured in steps of $\Delta t = 1$, and distances are scaled such that key quantities like diffusion coefficients and memory strengths remain of order unity.

V. BENCHMARKS AGAINST CLASSICAL MODELS

Figure 2 highlights the distinct dynamical signatures of classical and memory-driven models. In BM, FBM, and uncoupled GLE, particles A and B follow uncorrelated, isotropic motion, with MSDs that remain clearly separated across all lag times [Fig. 2(a)]. In our GLE implementation, we introduce a shared colored noise source to mimic a common viscoelastic environment. This shared stochastic background induces mild temporal alignment between particles, causing their trajectories and diffusion exponents to drift closer over time—even in the absence of explicit coupling. This results in a small but nonzero coherence $C_{AB}(\tau)$ and narrowing of the gap between $\alpha_A(\tau)$ and $\alpha_B(\tau)$ [Figs. 2(b) and 2(c)]. All simulations begin at $t = 0$ with particles initialized at the origin, and memory convolution terms are computed from this starting point, with no prior history assumed.

In MechGLE, we initialize particles A and B with distinct memory exponents—γ_A and γ_B—which govern the power-law decay of their respective memory kernels (e.g., $\gamma_A = 0.8$ and $\gamma_B = 1.9$), to examine how quickly mechanical coupling drives dynamical convergence. Owing to the symmetric nature of their coupling through a mechanical spring, this convergence occurs rapidly, with both particles soon exhibiting identical effective dynamics—a hallmark of conservative, symmetry-enforcing interactions. Although high temporal coherence can be achieved in both GLE and MechGLE by suitable parameter tuning, it invariably comes at the cost of losing diffusive heterogeneity. In MechGLE, any coherence is only transient—symmetry in the coupling eventually forces both particles into the same diffusive state. This intrinsic tradeoff, rooted in the reciprocal coupling structure, highlights a fundamental limitation of these models in sustaining coherent yet distinct dynamical behaviors.

By contrast, the CMGP framework preserves dynamical disparity while maintaining sustained coherence. Despite persistent differences between $\alpha_A(\tau)$ and $\alpha_B(\tau)$, the cross correlation $C_{AB}(\tau)$ remains high. This coexistence of coherence without convergence defines the regime of ghost coherence, which arises through asymmetric, memory-mediated interactions [35,36]—a hallmark of CMGP dynamics that closely parallels the "anomalous yet Brownian" diffusion scenario [37]. We also compare GLE, MechGLE, and CMGP under isolated versus common noise (Fig. S4 in Supplemental Material [38]): with isolated noise, only CMGP sustains appreciable long-lag coherence, whereas GLE/MechGLE remain near zero; adding a shared component increases $C_{AB}(\tau)$ in all models, chiefly via common-drive correlations in GLE/MechGLE, while CMGP continues to exhibit ghost coherence without enforcing trajectory convergence. Asymmetric coupling phenomena—such as leader-follower synchronization [39] or directed percolation [40]—capture aspects of one-way influence but typically produce full dynamical convergence or static transitions; likewise, noise-induced synchronization of identical stochastic dynamics [34] forces trajectories to converge under common noise. In contrast, CMGP uniquely supports high temporal coherence while preserving persistent dynamical disparity. Finally, the CMGP coherence curves often exhibit an initial negative dip [e.g., $C_{AB}(1) \approx -0.5$ in our parametrization], reflecting a finite-memory latency: at very small lags particle A has not yet integrated informative increments from B, yielding a transient phase mismatch. As B begins to move and A integrates its history, coherence builds through memory accumulation. Thus, ghost coherence here is fundamentally mimetic rather than "genetic"—an emergent alignment shaped by ongoing dynamics, not preset symmetry.

VI. PARAMETER DEPENDENCE AND REGIMES

Figure 3 compares two realizations of the CMGP model that demonstrate persistent directional coherence despite contrasting spatial trajectories, driven by different balances between coupling strength (κ) and memory depth (M). In the top row ($\kappa > M$), the active particle A maintains a lo-

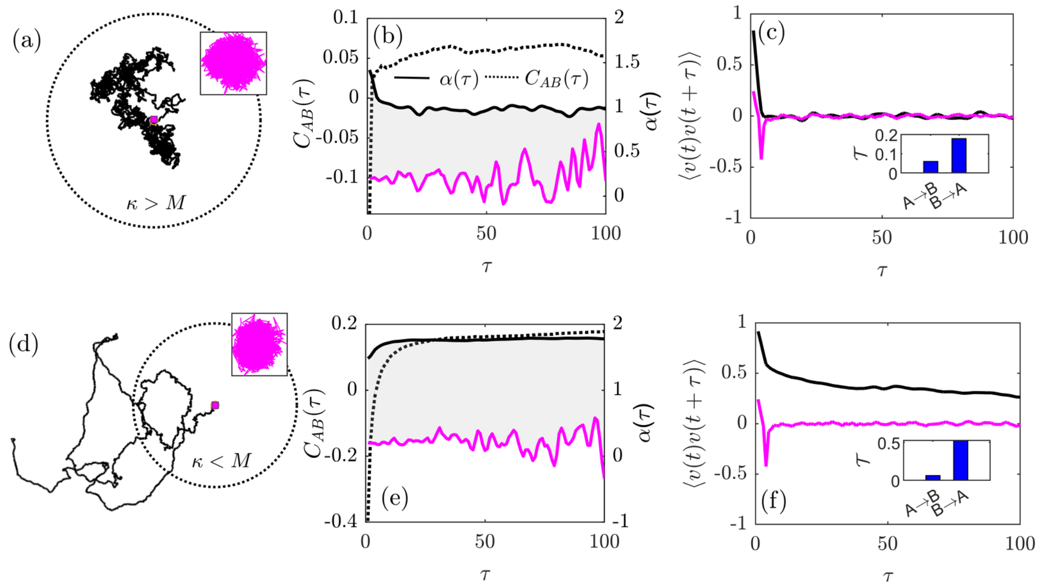

FIG. 3. Representative CMGP realizations illustrating how the balance between coherence strength κ and memory depth M shapes trajectory structure and interparticle dynamics. (a), (d) Trajectories of active particle A (black) and passive particle B (magenta); inset: zoom on passive motion. Top row: $\kappa > M$ ($\kappa/M = 10$, $R = 150$) regime; bottom row: $\kappa < M$ ($\kappa/M = 0.1$, $R = 600$) regime. (b), (e) Cross coherence $C_{AB}(\tau)$ and local diffusion exponents $\alpha(\tau)$ reveal persistent directional alignment in both cases, with greater disparity in α when memory dominates. (c), (f) Velocity autocorrelation functions $\langle v(t)v(t+\tau)\rangle$ and transfer entropy [41] bar plots confirm consistent unidirectional information flow from the passive to active particle, despite markedly different spatial and temporal signatures. In panels (a), (d), the dashed circle has radius R, i.e., the coupling decay length used in $K(d) = \kappa\, e^{-d/R}$. It is a visual reference only; no confining potential or boundary is imposed. Trajectories evolve in free space and may wander outside this circle. Instantaneous influence scales with separation via $K(d)$, and the observed long-lag coherence reflects memory and intermittent proximity rather than confinement.

calized and temporally consistent trajectory, whereas in the bottom row ($\kappa < M$), A exhibits broader spatial wandering. In both cases, the passive particle B remains confined, and the overall cross correlation $C_{AB}(\tau)$ [panels (b) and (e)] remains high—indicating that coherent alignment persists independent of visual or geometric similarity. Panels (c) and (f) present the velocity autocorrelation functions (VACF), $\langle v(t)v(t+\tau)\rangle$, which reveal long-term temporal structure in A's motion, particularly when its memory dominates (i.e., large M). Transfer entropy [41], defined as the excess uncertainty reduction in predicting the future of particle j given the past of particle i beyond the past of j itself, quantifies the directed information flow between coupled dynamics. Mathematically, it is given by $\mathcal{T}_{i\to j} = \sum p(x_j^{t+1}, x_j^t, x_i^t)\log(\frac{p(x_j^{t+1}|x_j^t,x_i^t)}{p(x_j^{t+1}|x_j^t)})$, where $p(\cdot)$ denotes joint probabilities. Here, log denotes $\log_2$, so transfer entropy is reported in bits (using natural logs would report nats and scale values by $\ln 2$). Despite symmetric mechanical coupling, the observed transfer entropy $\mathcal{T}_{i\to j}$ (insets) consistently exhibits a pronounced asymmetry: $\mathcal{T}_{B\to A} \gg \mathcal{T}_{A\to B}$, confirming that the effective information flow is predominantly unidirectional. Notably, the asymmetry is amplified when particle A preserves its internal persistence: when memory dominates, A retains its own scaling ("dynamic integrity") while becoming more susceptible to informative input from B without directly mirroring B's trajectory (ghost coherence). Influence is strictly distance gated via $K(d)$; consequently, if the pair remains far apart ($d \gg R$) for durations exceeding the memory window M, the coupling term effectively vanishes and $C_{AB}(\tau)$ decays accordingly. Our intent is to demonstrate long-lag coherence sustained by the combination of memory and intermittent proximity, not persistent influence at infinite separation.

The CMGP dynamics resemble a kite loosely tethered to a jittery pillar: although the kite appears free, its coherent motion subtly encodes the pillar's fluctuations. Attempts by the kite to control the anchor disrupt coherence, whereas passive adherence enables it to act as an ideal information carrier, persistently encoding the partner's dynamics. This highlights how asymmetry fosters functional coherence: the more persistently A preserves its own behavior, the more effectively it transmits information from B. Thus, CMGP reveals a nonreciprocal coordination mechanism, where persistent self-dynamics coexist with directional informational guidance, challenging classical notions of mutual interaction.

To identify regimes where coherence and persistence coexist, we employed Bayesian optimization [42] to maximize the state persistence index ($\mathcal{SPI}$), defined as $\mathcal{SPI} = 1 - \mathrm{std}(\alpha_A)$, over the CMGP parameter space (κ, M, R, H_B). Treating the $\mathcal{SPI}$ landscape as a posterior distribution $p(\mathcal{SPI} \mid \kappa, M, R, H_B)$, new evaluations were selected by optimizing an acquisition function balancing exploration (uncertainty) and exploitation (predicted gain). Figure 4 shows Bayesian-smoothed parameter maps of $\mathcal{SPI}$ over (κ, M) for varying (R, H_B). As R increases and H_B decreases ($H_B \lesssim 0.3$), broader stability zones emerge, confirming the "kite" intuition: spatial freedom enhances dynamic self-consistency while maintaining directional coherence. Thus, robust coherence persists across a wide parameter swath without fine

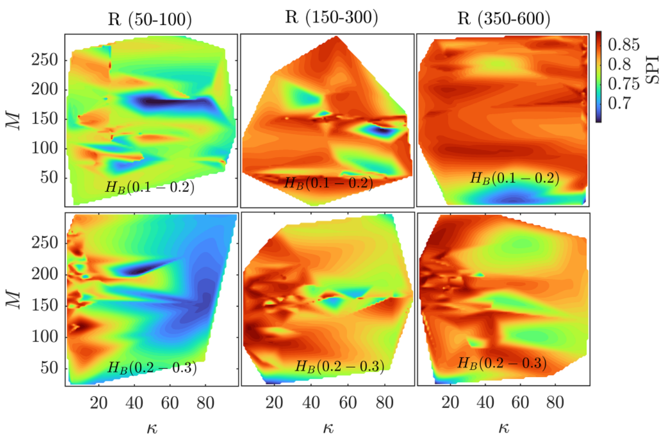

FIG. 4. Parameter landscapes of the state persistence index ($\mathcal{SPI}$) across the CMGP parameter space: $\mathcal{SPI}$ is defined as $1 - \mathrm{std}(\alpha_A)$, quantifying the temporal consistency of the active particle's local scaling exponent. Each panel displays $\mathcal{SPI}$ as a function of coupling strength κ and memory depth M, across varying ranges of confinement radius R (columns) and passive Hurst exponent H_B (rows). Warmer colors indicate more stable (persistent) motion of the active agent, while cooler regions reflect dynamic instability. The results demonstrate that sufficient mechanical space (R) enables A to sustain coherent dynamics while maintaining responsiveness to the subdiffusive background B.

tuning, arising from constructive memory-coupling interplay under spacious confinement.

VII. CONCLUSIONS

Building on these parameter landscapes, we show that particles with distinct diffusive identities can sustain long-time temporal coherence without trajectory symmetry, reciprocity, or mechanical consensus. Robust regions of the CMGP space yield "ghost" coherence—alignment in time without spatial colocalization—because relational memory and directed, distance-gated coupling integrate information across intermittent encounters. In heterogeneous and disordered settings, visual proximity is therefore a poor proxy for synchrony, and the observed asymmetry in transfer entropy demonstrates that influence can be strongly directional yet functionally meaningful. A system-specific quantitative validation (e.g., chromatin loci, telomeres, peroxisomes) is beyond the scope of this study. We view this as a natural direction for future—or collaborative—work: testing CMGP's falsifiable signatures on curated cotracking datasets with calibrated localization error and drift controls, and extending the framework to multinode networks, adaptive or nonexponential gains, and time-varying memory. More broadly, CMGP offers a route to modeling heterogeneous, memory-rich systems in which coherence is not imposed but self-organized, with implications for intracellular transport and for the design of synthetic active materials.

ACKNOWLEDGMENTS

The author gratefully acknowledges Prof. Matthias Weiss (University of Bayreuth, Germany) and Prof. Manoj Kumbhakar (BARC, India) for their valuable encouragement, insightful discussions, and continued support.This work received financial and institutional support from the Bhabha Atomic Research Centre, Department of Atomic Energy, Government of India. Additional institutional support was provided by the University of Bayreuth, Germany.

DATA AVAILABILITY

The data are not publicly available. The data are available from the authors upon reasonable request.

[1] A. V. Ratushny, R. A. Saleem, K. Sitko, S. A. Ramsey, and J. D. Aitchison, Asymmetric positive feedback loops reliably control biological responses, Mol. Syst. Biol. **8**, 577 (2012).

[2] N. Levernier, O. Bénichou, R. Voituriez, and T. Guérin, Kinetics of rare events for non-Markovian stationary processes and application to polymer dynamics, Phys. Rev. Res. **2**, 012057 (2020).

[3] M. Weiss, M. Elsner, F. Kartberg, and T. Nilsson, Anomalous subdiffusion is a measure for cytoplasmic crowding in living cells, Biophys. J. **87**, 3518 (2004).

[4] R. Metzler and J. Klafter, The random walk's guide to anomalous diffusion: A fractional dynamics approach, Phys. Rep. **339**, 1 (2000).

[5] E. Barkai, Y. Garini, and R. Metzler, Strange kinetics of single molecules in living cells, Phys. Today **65**, 29 (2012).

[6] I. M. Sokolov, Models of anomalous diffusion in crowded environments, Soft Matter **8**, 9043 (2012).

[7] N. Fakhri, A. D. Wessel, C. Willms, M. Pasquali, D. R. Klopfenstein, F. C. MacKintosh, and C. F. Schmidt, Long-range correlated motion in the cytoplasm of living cells, Science **344**, 1031 (2014).

[8] B. G. Mitterwallner, C. Schreiber, J. O. Daldrop, J. O. Rädler, and R. R. Netz, Non-Markovian data-driven modeling of single-cell motility, Phys. Rev. E **101**, 032408 (2020).

[9] Y. Qiu, R. P. Wiewiora, J. A. Izaguirre, H. Xu, W. Sherman, W. Tang, and X. Huang, Non-Markovian dynamic models identify non-canonical KRAS-VHL encounter complex conformations for novel PROTAC design, JACS Au **4**, 3857 (2024).

[10] B. B. Mandelbrot and J. W. V. Ness, Fractional Brownian motions, fractional noises and applications, SIAM Rev. **10**, 422 (1968).

[11] J.-H. Jeon, V. Tejedor, S. Burov, E. Barkai, C. Selhuber-Unkel, K. Berg-Sørensen, L. B. Oddershede, and R. Metzler, *In vivo* anomalous diffusion and weak ergodicity breaking of lipid granules, Phys. Rev. Lett. **106**, 048103 (2011).

[12] S. C. Kou and X. S. Xie, Generalized langevin equation with fractional Gaussian noise: Subdiffusion within a single protein molecule, Phys. Rev. Lett. **93**, 180603 (2004).

[13] E. Lutz, Fractional Langevin equation, Phys. Rev. E **64**, 051106 (2001).

[14] E. Barkai, Aging in subdiffusion generated by a deterministic dynamical system, Phys. Rev. Lett. **90**, 104101 (2003).

[15] J.-H. Jeon and R. Metzler, Noisy continuous time random walks, J. Phys. A: Math. Theor. **46**, 345002 (2013).

[16] D. Mizuno, C. Tardin, C. F Schmidt, and F. C MacKintosh, Nonequilibrium mechanics of active cytoskeletal networks, Science **315**, 370 (2007).

[17] L. Onsager, Reciprocal relations in irreversible processes. I, Phys. Rev. **37**, 405 (1931).

[18] F. Höfling and T. Franosch, Anomalous transport in the crowded world of biological cells, Rep. Prog. Phys. **76**, 046602 (2013).

[19] A. Caspi, R. Granek, and M. Elbaum, Enhanced diffusion in active intracellular transport, Phys. Rev. Lett. **85**, 5655 (2000).

[20] I. Golding and E. C. Cox, Physical nature of bacterial cytoplasm, Phys. Rev. Lett. **96**, 098102 (2006).

[21] S. C Weber, A. J Spakowitz, and J. A Theriot, Nonthermal atp-dependent fluctuations contribute to the in vivo motion of chromosomal loci, Proc. Natl. Acad. Sci. USA **109**, 7338 (2012).

[22] P. Dieterich, R. Klages, R. Preuss, and A. Schwab, Anomalous dynamics of cell migration, Proc. Natl. Acad. Sci. USA **105**, 459 (2008).

[23] T. J. Lampo, S. Stylianidou, M. P. Backlund, P. A. Wiggins, and A. J. Spakowitz, Cytoplasmic rna-protein particles exhibit non-gaussian subdiffusive behavior, Biophys. J. **112**, 532 (2017).

[24] I. Goychuk, Viscoelastic subdiffusion: From anomalous to normal, Phys. Rev. E **86**, 021113 (2012).

[25] R. Kupferman, Fractional kinetics in Kac-Zwanzig heat bath models, J. Stat. Phys. **114**, 291 (2004).

[26] Z. Li, H. S. Lee, E. Darve, and G. Em Karniadakis, Computing the non-Markovian coarse-grained interactions derived from the Mori–Zwanzig formalism in molecular systems: Application to dissipative particle dynamics, J. Chem. Phys. **146**, 014104 (2017).

[27] G. Jung, M. Hanke, and F. Schmid, Generalized Langevin dynamics: Construction and numerical integration of non-Markovian particle-based models, Soft Matter **14**, 9368 (2018).

[28] T. J. Doerries, S. A. M. Loos, and S. H. L. Klapp, Correlation functions of non-Markovian systems out of equilibrium: Analytical expressions beyond single-exponential memory, J. Stat. Mech. (2021) 033202.

[29] A. Zidovska, D. A. Weitz, and T. J. Mitchison, Micron-scale coherence in interphase chromatin dynamics, Proc. Natl. Acad. Sci. USA **110**, 15555 (2013).

[30] M. Hidalgo-Soria, Y. Haddad, E. Barkai, Y. Garini, and S. Burov, Directed motion and spatial coherence in the cell nucleus, arXiv:2407.08899.

[31] C.-M. Svensson, K. Reglinski, W. Schliebs, R. Erdmann, C. Eggeling, and M. T. Figge, Quantitative analysis of peroxisome tracks using a hidden Markov model, Sci. Rep. **13**, 19694 (2023).

[32] M. Magdziarz, A. Weron, K. Burnecki, and J. Klafter, Fractional Brownian motion versus the continuous-time random walk: A simple test for subdiffusive dynamics, Phys. Rev. Lett. **103**, 180602 (2009).

[33] J. R. Gomez-Solano, A. Blokhuis, and C. Bechinger, Dynamics of self-propelled Janus particles in viscoelastic fluids, Phys. Rev. Lett. **116**, 138301 (2016).

[34] S. Fahy and D. R. Hamann, Transition from chaotic to nonchaotic behavior in randomly driven systems, Phys. Rev. Lett. **69**, 761 (1992).

[35] P. J. Daniell, The theory of functionals, and of integral and integro-differential equations. By Vito Volterra. Translated by M. Long. Pp. x + 226. 25s. 1930. (Blackie), The Mathematical Gazette **16**, 59 (1932).

[36] R. Kubo, The fluctuation-dissipation theorem, Rep. Prog. Phys. **29**, 255 (1966).

[37] M. V. Chubynsky and G. W. Slater, Diffusing diffusivity: A model for anomalous, yet Brownian, diffusion, Phys. Rev. Lett. **113**, 098302 (2014).

[38] See Supplemental Material at http://link.aps.org/supplemental/10.1103/6r83-n97h for detailed derivations of the CMGP model, extended simulation results, supporting discussions, and additional figures.

[39] A. Jadbabaie, J. Lin, and A. S. Morse, Coordination of groups of mobile autonomous agents using nearest neighbor rules, IEEE Trans. Autom. Contr. **48**, 988 (2003).

[40] H. Hinrichsen, Non-equilibrium critical phenomena and phase transitions into absorbing states, Adv. Phys. **49**, 815 (2000).

[41] T. Schreiber, Measuring information transfer, Phys. Rev. Lett. **85**, 461 (2000).

[42] D. J. C. MacKay, *Information Theory, Inference, and Learning Algorithms* (Cambridge University Press, Cambridge, 2003).